ChemPubSoc Europe

DOI: 10.1002/chem.201405261

CHEMISTRY
A European Journal
Full Paper

Molecular Photosensitizers

# Tris-Heteroleptic Ruthenium–Dipyrrinate Chromophores in a Dye-Sensitized Solar Cell

Guocan Li,[a] Ke Hu,[b] Kiyoshi C. D. Robson,[c] Serge I. Gorelsky,[d] Gerald J. Meyer,*[b] Curtis P. Berlinguette,*[c] and Michael Shatruk*[a]

**Abstract:** Two novel tris-heteroleptic Ru–dipyrrinates were prepared and tested as sensitizers in the dye-sensitized solar cell (DSSC). Under AM 1.5 sunlight, DSSCs employing these dyes achieved power conversion efficiencies (PCEs) of 3.4 and 2.2%, substantially exceeding the value achieved previously with a bis-heteroleptic dye (0.75%). As shown by electrochemical measurements and DFT calculations, the improved PCEs stem from the synthetically tuned electronic structure, which affords more negative excited state redox potentials and favorable electron injection into the $TiO_2$ conduction band. Electron injection was quantified by nanosecond transient absorption spectroscopy, which revealed that the highest injection yield is achieved with the dye that acts as the strongest photoreductant.

## Introduction

In the last two decades, dye-sensitized solar cells (DSSCs) have emerged as an alternative strategy to generate electricity from solar light in a more feasible and economic fashion as compared to conventional photovoltaic technologies.[1] In a DSSC device, the absorption of a photon promotes the dye molecule to the excited state, from which an electron is injected into the conduction band of a mesoporous nanocrystalline wide band-gap semiconductor (usually $TiO_2$); the oxidized dye molecule is subsequently regenerated by a redox mediator, to complete the electric circuit. DSSC devices offer low cost, ease of fabrication, adaptability to flexible substrates, and high tolerance to impurities. These merits notwithstanding, the DSSCs still are not competitive in the global solar cell market due to the relatively low power conversion efficiency (PCE) and perceived stability issues. A large body of research on DSSCs have afforded a series of remarkable Ru-based dyes with PCE > 10%.[2] The first of them, $[Ru(dcbpy)_2(NCS)_2]$ (dcbpy = 4,4′-dicarboxylato-2,2′-bipyridine),[2a] was discovered by Grätzel, and subsequently used as a prototype to develop other dyes by substituting one dcbpy ligand with various derivatives of bpy, which allowed tuning the energy-level alignment and managing electron-transfer kinetics in the DSSC. These dyes perform well in the DSSCs, but they suffer from the presence of two labile $NCS^-$ ligands that may lower the stability of the dyes under operational conditions, that is, under illumination and thermal stress. These issues call for the exploration of highly efficient Ru sensitizers devoid of monodentate ligands.

In order to overcome this problem, a number of promising NCS-free Ru sensitizers have been explored in recent years.[3] Among the dyes of this class are Ru–dipyrrinate complexes (Scheme 1) that we recently explored as panchromatic sensitizers in DSSCs.[4,5] The anionic dipyrrinate ligand caught our attention for two reasons: 1) its substitution for the two $NCS^-$ ligands in the Ru complex not only preserves the position of the MLCT absorption but also increases the extinction coeffi-

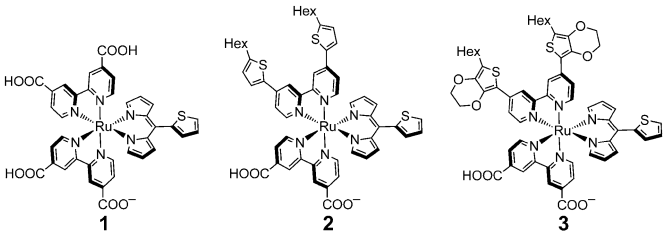


1 2 3

**Scheme 1.** Molecular structures of Ru–dipyrrinate dyes **1**–**3**.

[a] G. Li, Prof. M. Shatruk
Department of Chemistry and Biochemistry
Florida State University, Tallahassee, FL 32310 (USA)
E-mail: shatruk@chem.fsu.edu

[b] K. Hu, Prof. G. J. Meyer[+]
Department of Chemistry and Materials Science and Engineering
Johns Hopkins University
3400 North Charles Street, Baltimore, MD, 21218 (USA)

[c] K. C. D. Robson, Prof. C. P. Berlinguette[++]
Department of Chemistry and the Centre for Advanced Solar Materials
University of Calgary, Calgary AB, T2N 1N4 (Canada)

[d] Prof. S. I. Gorelsky
Centre for Catalysis Research and Innovation, Department of Chemistry
University of Ottawa, Ottawa, ON K1N 6N5 (Canada)

[+] Present Address:
Department of Chemistry, University of North Carolina at Chapel Hill
Chapel Hill, NC 27599 (USA)
E-mail: gjmeyer@email.unc.edu

[++] Present Address:
Department of Chemistry, University of British Columbia
Vancouver, BC V6T 1Z1 (Canada)
E-mail: gjmeyer@email.unc.edu

Supporting information for this article is available on the WWW under http://dx.doi.org/10.1002/chem.201405261.

cient; and 2) the dipyrrin moiety itself is an excellent chromophore with a characteristic self-absorption band at about 470 nm, which is complementary to the MLCT band. Thus, the incorporation of dipyrrinate greatly enhances the absorptivity of the Ru sensitizer, which allows the use of a thinner $TiO_2$ substrate to suppress the loss of electrons due to charge recombination. The synthetic chemistry of dipyrrins is also well-established,[6] thus offering a versatile platform to finely tune the electronic structures, as well as the electrochemical and photophysical properties of Ru–dipyrrinate complexes as dictated by the operational requirements of the DSSC.

These promising features of Ru–dipyrrinate complexes did not render the desired DSSC performance, as cells fabricated with [Ru($H_2$dcbpy)(Hdcbpy)(2-tdp)] (**1**, 2-tdp = 5-(2-thienyl)dipyrrinate) showed quite low PCEs of 1.3%. Our study of electron-transfer dynamics for the 3-thienyl-substituted analogue of **1** on mesoporous $TiO_2$ electrode showed the lowest excited state to lie merely 170 mV above the $TiO_2$ conduction band. Thus, these complexes are weak photoreductants, which might account for the low PCE values.[5] In order to overcome this problem, we prepared two derivatives of **1** by replacing one $H_2$dcbpy ligand with bis(2-thienyl-5-hexyl)-2,2′-bipyridine (dthbpy) or bis(2-thienyl-3,4-ethylenedioxo-5-hexyl)-2,2′-bipyridine (EDOT-bpy). These electron-donating substituents serve to destabilize the excited states in [Ru(Hdcbpy)(dthbpy)(2-tdp)] (**2**) and [Ru(Hdcbpy)(EDOT-bpy)(2-tdp)] (**3**), respectively, making these complexes better photoreductants than **1**. In addition, the more extended conjugation systems of the ligands enhance the absorptivity while the long hydrophobic hexyl chains help to suppress charge recombination processes between the electrolyte and $TiO_2$ and to prevent water from reaching the surface and desorbing the dye molecules. These features should render **2** and **3** better DSSC sensitizers than **1**.

In this contribution, we report the synthesis and characterization of dyes **2** and **3** and their DSSC performance. The PCEs of the cells prepared with **2** and **3** are significantly higher than the value observed with **1**. The injection yield and dye regeneration kinetics were investigated by nanosecond transient absorption spectroscopy to provide insights into the underlying mechanisms that govern the cell efficiency. To the best of our knowledge, this report provides the first use of tris-heteroleptic Ru–dipyrrinate complexes as sensitizers in DSSCs.

## Results and Discussion

### Synthesis

The synthesis of tris-heteroleptic Ru complexes is challenging, and a general synthetic protocol toward such complexes does not currently exist.[7] Inspired by the synthesis of such a complex with phenylpyridine (ppy),[3b,8] which used a $[Ru(ppy)(CH_3CN)_4]^+$ precursor, we applied a similar approach to create a precursor that would contain one dipyrrinate and four $CH_3CN$ ligands around the Ru center. The synthesis began with 5-(2-thienyl)-dipyrromethane, which was oxidized to 2-tdp by DDQ (Scheme 2). The obtained product, without further purification, was reacted with [{$RuCl_2$(*p*-cymene)}$_2$] in the presence of $Et_3N$ to obtain [Ru(*p*-cymene)(2-tdp)Cl]. Refluxing the latter with $AgNO_3$ in $CH_3CN$ for three days led to [Ru(2-tdp)$(CH_3CN)_4$]$NO_3$ in 86% yield. Afterwards, a 4,4′-bis(ethoxycarbonyl)-2,2′-bipyridine (deeb) ligand was coordinated to the Ru center by replacing two labile $CH_3CN$ ligands, since the corresponding product can be used for preparing both **2** and **3**. The reaction was performed in EtOH at 55 °C for 30 h. The temperature of this step is critical, as the reaction proceeds very slowly below 40 °C, but [Ru(deeb)$_2$(2-tdp)]$NO_3$ becomes the major product if the temperature is too high (e.g., reflux). The obtained [Ru(deeb)(2-tdp)$(CH_3CN)_2$]$NO_3$ was a mixture of *cis*- and *trans*- isomers with the latter prevailing according to the $^1$H NMR spectrum (see the Supporting Information). In the case of $[Ru(bpy)(ppy)(CH_3CN)_2]^+$, however, the *cis*-isomer was favored.[8] The structural difference is probably caused by the six-membered metallocycle formed upon coordination of 2-tdp as compared to the five-membered metallocycle for coordinated ppy. This feature moves the pyrrolic α-proton of 2-tdp closer to the adjacent bpy ligand in the *cis*-geometry, but such a steric effect is not present in the *trans*-isomer. Finally, [Ru(deeb)(2-tdp)$(CH_3CN)_2$]$NO_3$ was reacted with dthbpy or EDOT-bpy under reflux to afford ester derivatives **2a** and **3a**, respectively. Hydrolysis of the ester derivatives in a DMF:$Et_3N$:$H_2O$ mixture (3:1:1 v/v/v) gave rise to dyes **2** and **3**. Similar to the ppy derivatives, elemental analysis revealed that the dyes were obtained as neutral zwitterions due to deprotonation of one of the carboxylic groups.

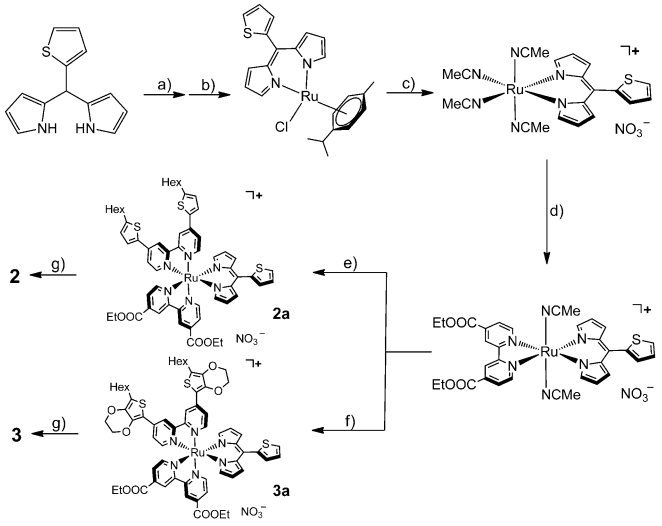


**Scheme 2.** a) DDQ, THF, RT, 1 h; b) [{$RuCl_2$(*p*-cymene)}$_2$], $Et_3N$, $CH_3CN$, reflux, 12 h, 70%; c) $AgNO_3$, $CH_3CN$, reflux, 3 days, 86%; d) deeb, EtOH, 55 °C, 30 h, 48%; e) dthbpy, EtOH, reflux, 12 h, 80%; f) EDOT-bpy, EtOH, reflux, 12 h, 90%; g) $Et_3N$:$H_2O$:DMF = 1:1:3, reflux, 18 h, 84% for **2** and 91% for **3**.

### Electronic structure

In order to examine the electronic structures of frontier molecular orbitals (MOs), density-functional theory (DFT) calculations were performed on optimized geometries of complexes **1** and **2** using the B3LYP functional and the TZVP basis set (DZVP for Ru) (Figure 1). To make the calculations less time-demanding,

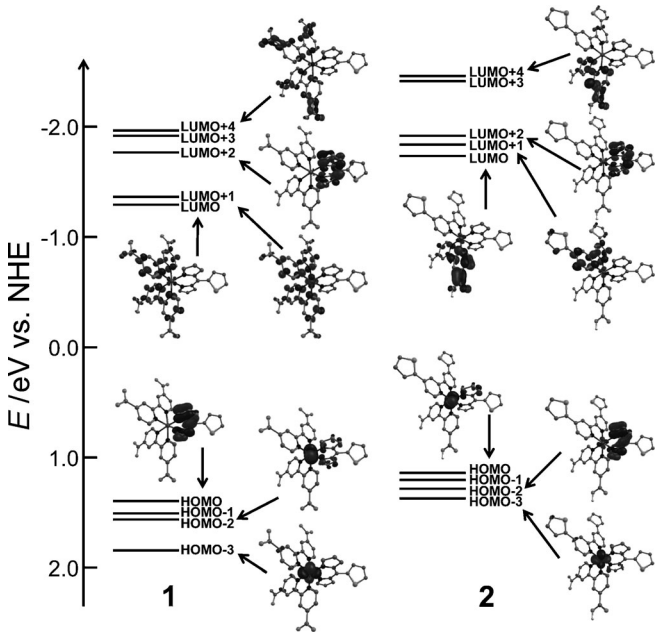


**Figure 1.** Selected frontier molecular orbitals of **1** and **2**. Isosurface contour values are 0.05 a.u. H atoms are omitted for clarity.

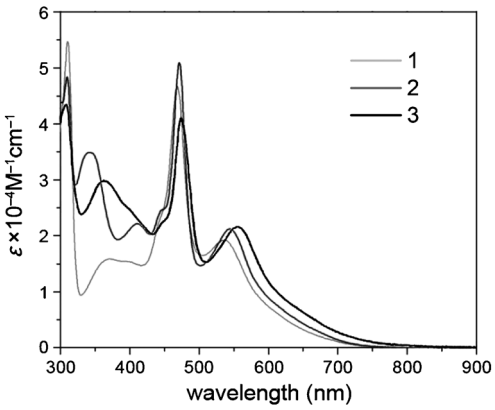


**Figure 2.** Optical absorption spectra of the fully deprotonated forms of **1** (light gray), **2** (gray), and **3** (black) collected in basic $CH_3OH$ at room temperature.

hexyl groups in **2** were substituted with H atoms, which should not cause a significant change to the nature and energy of frontier orbitals. In **1**, the highest-occupied molecular orbital (HOMO) is localized on dipyrrinate, and three metal-centered (Ru 4d) MOs appear below the HOMO. In **2**, both HOMO and HOMO−1 are Ru-based, while HOMO−2 is localized on the dipyrrinate ligand. The lowest-unoccupied molecular orbitals (LUMOs) are similar in both complexes and are mainly localized on dcbpy, except for LUMO+2 which is dipyrrinate-centered. We note that all the frontier MOs of **2** are shifted to higher energy relative to the analogous orbitals of **1**. The destabilization of the orbitals is consistent with the presence of electron-donating thienyl substituents in **2** instead of the electron-withdrawing carboxylates in one of the bpy-based ligands in **1**. The change in the substituent has a stronger effect on the energies of the Ru-based MOs than on the energies of the orbitals localized on the more distant dipyrrinate ligand. Consequently, the Ru d-orbitals surpass the dipyrrinate π-orbital and become the HOMO and HOMO−1 in **2**. More importantly, the destabilization of the bpy-centered LUMOs renders **2** a better photoreductant, which links back to our initial objective formulated in the introduction. Although DFT calculations were not performed for **3**, the even more electron-donating EDOT substituents should further destabilize the MOs of this complex relative to the MOs of **2**.

### Optical absorption spectroscopy

The UV/Vis absorption spectra of **1**, **2**, and **3** were recorded in $CH_3OH$ (Figure 2). Two equivalents of $(Bu_4N)OH$ were added to assure the full dissolution and to accurately measure the extinction coefficients of the fully deprotonated complexes. The absorption spectra show similar features, including three distinct peaks around 300, 470, and 550 nm; TD-DFT calculations indicate these absorption bands to be a bpy π–π* transition, a dipyrrinate π–π* transition coupled to the intraligand charge transfer (ILCT) transition, and an MLCT transition, respectively.[4] Aside from these three major bands, an additional band at about 350 nm becomes pronounced in **2** and **3**. A bathochromic shift was observed for the MLCT band of **2** and **3** as compared to **1**, which is in good agreement with the changes in the MO energies established by the DFT calculations. The higher extinction coefficient of the MLCT bands in **2** and **3** can be attributed to the more delocalized π* LUMOs in these complexes. Such delocalization is known to enhance the absorptivity in molecular systems.[2b] Overall, the extinction coefficient of **2** and **3** is increased in the low-energy region. This feature should afford better harvesting of long-wavelength photons and increased efficiency of DSSCs. Just as other reported Ru–dipyrrinate complexes, neither **2** nor **3** shows luminescence at room temperature.[9] The general non-emissive behavior of these complexes can be attributed to a combination of the energy-gap effect (the non-radiative decay rate constant increases exponentially with decreasing the HOMO–LUMO energy gap)[10] and internal rotation of the *meso*-substituent, which was shown to efficiently deactivate the excited state in Zn–dipyrrinate chromophores.[11]

### Cyclic voltammetry

In order to experimentally prove that **2** and **3** are better photoreductants than **1**, electrochemical properties of their more soluble ester derivatives, **2a** and **3a**, were assessed by cyclic voltammetry (CV). Similar to **1a**, both **2a** and **3a** exhibit a quasi-reversible Ru-centered oxidation process and three ligand-based reversible reduction processes, which can be assigned to two $bpy^{0/-}$ and one $dipyrrinato^{0/-}$ redox couples, respectively (Figure 3). In comparison to **1a**, the $E_{1/2}$ values of **2a** and **3a** are shifted towards more negative values. This finding agrees with the DFT calculations that show the frontier MOs are shifted to higher energy in **2** and **3** as compared to **1**. Since the first reduction potential qualitatively correlates with

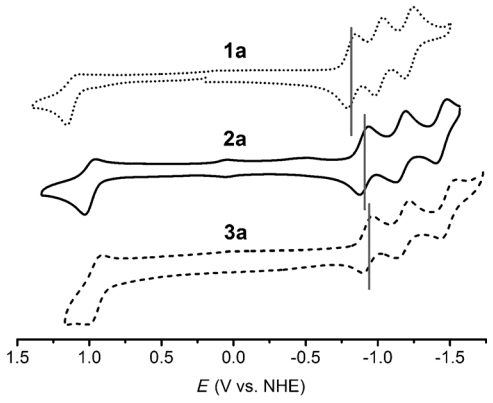


**Figure 3.** Cyclic voltammogram of **1a** (dotted line), **2a** (solid line), and **3a** (dashed line) collected in $CH_3CN$ with 0.1 M $(Bu_4N)PF_6$ as supporting electrolyte at room temperature.

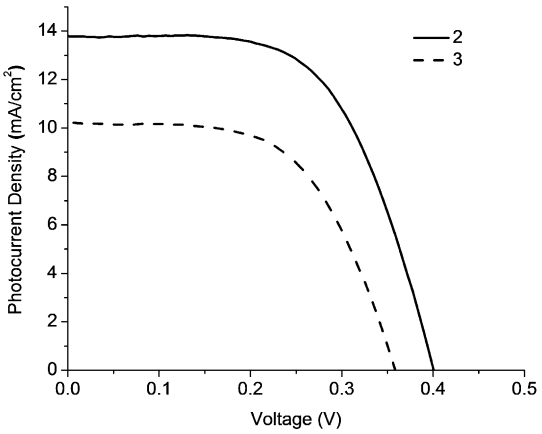


**Figure 4.** Photocurrent density–voltage curves of **2** (solid) and **3** (dashed) measured under irradiation of one sun.

the lowest excited state energy,[12] the electrochemical behavior of **2** and **3** confirms the increased excited-state energies in these complexes relative to the excited states of **1**. The CVs of **2** and **3** were obtained in DMF solution. They also exhibit a quasi-reversible oxidation process at 0.95 and 0.92 V, respectively (Figure S1 in the Supporting Information). The energy of the lowest excited state, $E(S^+/S^*)$, was calculated to be −0.70 V for **2** and −0.73 V for **3** using the equation $E_{S^*/S} = E_{S^+/S} - E_{0-0}$, in which $E_{S^+/S}$ is taken as the $E_{1/2}{}^{1+/0}$ redox potential (Table 1) of the complex and $E_{0-0}$ is determined as the onset of the optical absorption spectrum (1.65 V). Thus, for each complex, the HOMO energy is lower than the redox potential of the $I_2^{\bullet-}/I^-$ couple (+0.8(1) V),[13] while the lowest excited state lies above the bottom of the $TiO_2$ conduction band ($E_{cb} \sim -0.50$ V),[1] making these complexes viable DSSC sensitizers.

**Table 1.** Electrochemical properties of complexes **1**–**3** and **1a**–**3a** (the potentials are referenced to NHE).

| | Solvent | Half-wave potentials [V] | | | |
|---|---|---|---|---|---|
| | | $E_{1/2}{}^{1+/0}$ | $E_{1/2}{}^{0/1-}$ | $E_{1/2}{}^{1-/2-}$ | $E_{1/2}{}^{2-/3-}$ |
| **1a** | $CH_3CN$ | 1.11 | −0.82 | −1.04 | −1.28 |
| **2a** | $CH_3CN$ | 0.99 | −0.91 | −1.16 | −1.44 |
| **3a** | $CH_3CN$ | 0.95 | −0.93 | −1.18 | −1.49 |
| **1**[4] | DMF | 1.05 | | | |
| **2** | DMF | 0.95 | −1.10 | −1.37 | |
| **3** | DMF | 0.92 | −1.12 | | |

## DSSC performance

In order to examine the cell performance, **2** and **3** were anchored to mesoporous $TiO_2$ films, which consisted of a 12 μm thick transparent layer and 3 μm thick scattering layer. The dyes were applied to the films by dipping a blank $TiO_2$ slide in a $3 \times 10^{-4}$ M ethanolic solution of **2** or **3** for 16 h. In order to fully solubilize the dyes, two equivalents of $(Bu_4N)OH$ in EtOH were added to the dye solution. To provide the $I_3^-/I^-$ redox mediator, an electrolyte was prepared that contained 0.7 M LiI, 0.3 M DMII (1,3-dimethylimidazolium iodide), 0.06 M $I_2$, and 0.1 M GuSCN (guanidinium thiocyanate) in a mixture of acetonitrile and valeronitrile (85:15 v/v). The PCEs of these cells were measured under simulated AM 1.5 sunlight (Figure 4, Table 2). The cell containing dye **2** gave rise to an open-circuit voltage ($V_{oc}$) of 0.40 V, a short-circuit current density ($J_{sc}$) of 13.8 mA cm$^{-2}$, and a PCE of 3.4%, while the cell with dye **3** offered $V_{oc} = 0.36$ V, $J_{sc} = 10.2$ mA cm$^{-2}$, and PCE = 2.2%. In comparison to **1** under the same conditions (PCE = 0.75%),[4] the PCEs of DSSCs with dyes **2** and **3** have significantly improved. Indeed, dye **2** offers the highest PCE among all known dipyrrin-containing photosensitizers reported to date. Interestingly, the cell with **2** showed the higher $J_{sc}$ than the one with **3**, despite the higher excited state energy of the latter. We hypothesized that the smaller $J_{sc}$ value found with **3** could stem from a lower amount of this dye loaded onto the $TiO_2$ surface, taking into account the larger molecular size of **3** as compared to **2**. Such an effect was reported for other EDOT-containing Ru sensitizers.[14] A control experiment was performed by dipping two identical $TiO_2$ slides in solutions of **2** and **3** in ethanol at equal concentrations for 16 h. The resultant $TiO_2$ slides showed much stronger coloration in the case of dye **2** (Figure S2 in the Supporting Information). Since the extinction coefficients of both dyes are similar in the visible region (Figure 2), these observations suggest that a larger amount of **2** has been loaded on the $TiO_2$ surface, thus confirming our hypothesis.

**Table 2.** Photovoltaic characteristics of DSSCs containing sensitizers **2** and **3** under AM 1.5 illumination.

| | Active area [cm$^2$] | $J_{sc}$ [mA cm$^{-2}$] | $V_{oc}$ [V] | Fill factor | PCE [%] |
|---|---|---|---|---|---|
| **2** | 0.26 | 13.8 | 0.40 | 0.60 | 3.4 |
| **3** | 0.26 | 10.2 | 0.36 | 0.59 | 2.2 |

In order to gain more insights into the detailed parameters controlling the dye performance, nano-second transient absorption spectroscopy was applied to study the interfacial electron-transfer processes and dye regeneration behaviors of **2** and **3** on $TiO_2$ films.

### Injection yield measurements

Comparative actinometry was carried out using nanosecond transient absorption spectroscopy to quantify the relative excited state electron injection yields of **1**/$TiO_2$, **2**/$TiO_2$, and **3**/$TiO_2$. Figure 5 shows single-wavelength absorption changes

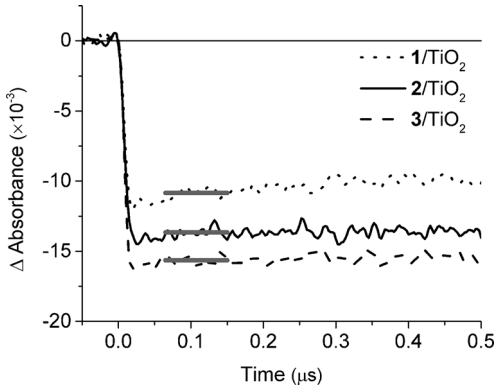


**Figure 5.** Absorption changes monitored at 550 nm for **1**/$TiO_2$ (dotted) and at 560 nm for **2**/$TiO_2$ (solid) and **3**/$TiO_2$ (dashed) after 532 nm pulsed laser excitation. Overlaid gray solid lines signify the MLCT bleach signals for injection yield calculations.

in 0.5 M $LiClO_4/CH_3CN$ solutions monitored at 550 nm for **1**/$TiO_2$ and at 560 nm for **2**/$TiO_2$ and **3**/$TiO_2$ after excitation with a 532 nm pulsed laser. The negative absorbance signal indicates the formation of oxidized dyes that absorb less light than their neutral forms in the ground states. The immediate appearance of the bleaching signal suggests that the oxidized molecules formed within the duration of the laser pulse. This is consistent with ultrafast excited state electron injection, $k_{inj} > 10^8\ s^{-1}$. The oxidized states live over a micro- to millisecond time period and finally recombine with the electrons injected into $TiO_2$. The transient absorption amplitudes observed immediately after the laser pulse were used to quantify the relative injection yields according to Equation (1), in which $\Delta$Abs is the transient absorption signal amplitude averaged for the period from 65 to 135 ns to exclude any possible excited state decay, $\Delta\varepsilon$ is the extinction coefficient difference between the oxidized and ground states of the dye (measured by spectroelectrochemistry, Figure S3 in the Supporting Information), $A$ is the absorptance of the ground state sensitizers at 532 nm excitation, and the subscripts s and r denote the sample and the reference, respectively.

$$\phi_{inj,s} = \frac{\Delta Abs_s \times \Delta\varepsilon_r \times A_r}{\Delta Abs_r \times \Delta\varepsilon_s \times A_s} \times \phi_r \qquad (1)$$

**Table 3.** Excited state injection yields measurement for **1**/$TiO_2$, **2**/$TiO_2$, and **3**/$TiO_2$ in 0.5 M $LiClO_4/CH_3CN$.

| | 1 | 2 | 3 |
|---|---|---|---|
| monitored wavelength [nm] | 550 | 560 | 560 |
| original $\varepsilon$ [$\times 10^{-4}$ M$^{-1}$ cm$^{-1}$] | 1.86 | 1.83 | 2.14 |
| $\varepsilon$ after oxidation [$\times 10^{-4}$ M$^{-1}$ cm$^{-1}$] | 0.46 | 0.39 | 0.66 |
| $\Delta\varepsilon$ [$\times 10^{-4}$ M$^{-1}$ cm$^{-1}$] | 1.40 | 1.45 | 1.48 |
| $\Phi_{inj}$[a] | 0.63 | 0.86 | 1 |

[a] The injection yield was normalized against **3**/$TiO_2$.

The injection yield results are summarized in Table 3. The injection yield for **3**/$TiO_2$ was approximately 16% higher than the yield for **2**/$TiO_2$ and 59% higher than that for **1**/$TiO_2$. The higher injection yield is in agreement with **3** being the strongest excited-state reductant, as confirmed by electrochemical measurements (Figure 3). The favorable shift in the excited state energy was achieved by the introduction of the electron-donating thienyl and EDOT substituents on the periphery of bpy in **2** and **3**, respectively.

### Sensitizer regeneration

It has been shown in the literature that the charge recombination between $TiO_2(e^-)$ and the oxidized dye can compete with the sensitizer regeneration in an operational DSSCs even with the champion Ru-based sensitizers.[15] The inefficient regeneration can lead to loss of the injected electrons and hence to lower $V_{oc}$ values. It is of interest to know whether the 40 mV lowering of $V_{oc}$ for **3**/$TiO_2$ versus **2**/$TiO_2$ is partly due to the less efficient sensitizer regeneration by the iodide-based electrolyte. The regeneration was quantified by using different concentrations of LiI in the electrolyte while maintaining the same concentration of $Li^+$ by adjusting the amount of $LiClO_4$. Laser excitation at 532 nm resulted in excited state electron injection. Diiodide ($I_2^{\bullet-}$) was observed as an oxidized iodide species in the electrolyte, and the regeneration step can be generally written as the reaction given in Equation (2).

$$[I^-, S^+/TiO_2] + I^- \rightarrow S/TiO_2 + I_2^{\bullet-}\ (S = \mathbf{2}\text{ or }\mathbf{3}) \qquad (2)$$

Figure 6a shows the MLCT bleach recovery monitored at 560 nm for **2**/$TiO_2$ and **3**/$TiO_2$ after 532 nm laser excitation at various iodide concentrations. The complete titration data are provided in Figure S4 in the Supporting Information. The charge recombination between $TiO_2(e^-)$ and the oxidized dye was slow in the absence of iodide and the decay lifetime extended from microseconds to hundreds of milliseconds. The decay kinetics were described by a Kohlraush–Williams–Watts (KWW) model [Eq. (3)].[16] An average rate constant approximated by the first moment was obtained from Equation (4). The charge recombination rate constants were calculated in this manner and found to be equal to 30(6) $s^{-1}$ for both **2** and **3**. The addition of iodide to the electrolyte led to the reduction of the oxidized dye after the electron injection and hence greatly speeded up the MLCT bleach recovery. This regeneration step needed several microseconds to complete at high

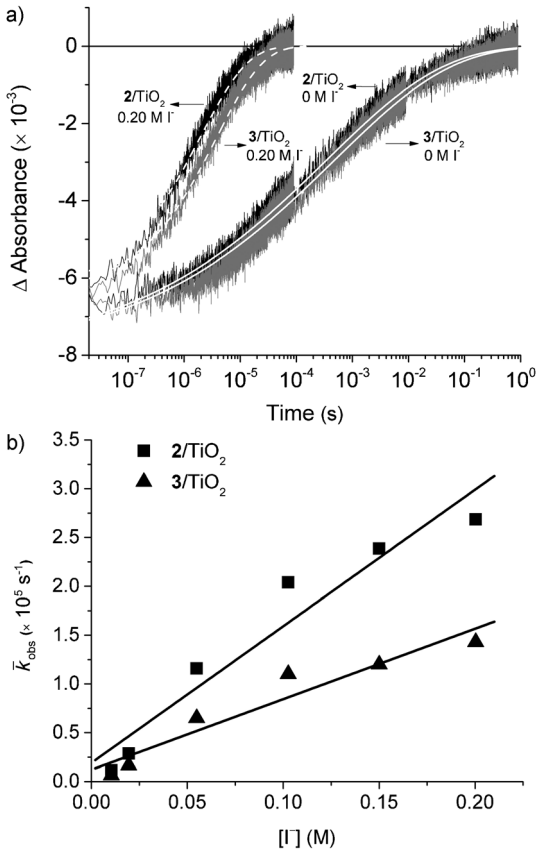


**Figure 6.** a) Absorbance monitored at 560 nm after 532 nm pulsed laser excitation of **2**/$TiO_2$ and **3**/$TiO_2$ at various concentrations of iodide in the electrolyte. Overlaid are the best kinetic fits for **2**/$TiO_2$ and **3**/$TiO_2$ in 0 M $I^-$ (solid white curves) and in 0.2 M $I^-$ (dashed white curves) based on KWW model as shown in Equation (3). b) Plot of observed average rate constant abstracted from Equation (4) versus the titrated iodide concentration.

**Table 4.** Rate constants for the regeneration of $\mathbf{2}^+$/$TiO_2$ and $\mathbf{3}^+$/$TiO_2$ after electron injection from the excited state of the dye.

| Dye | **2**/$TiO_2$ | **3**/$TiO_2$ |
|---|---|---|
| $k_{reg}$ [$M^{-1}s^{-1}$] | $1.4\times10^6$ | $7.2\times10^5$ |

concentration of iodide, and KWW model was again necessary to satisfactorily describe the data. A plot of the observed rate constants as a function of iodide concentration is shown in Figure 6b. The slope of a linear fit gave the second-order rate constants for the sensitizer regeneration, $k_{reg}=1.4\times10^6$ $M^{-1}s^{-1}$ and $7.2\times10^6$ $M^{-1}s^{-1}$ for **2**/$TiO_2$ and **3**/$TiO_2$, respectively.

$$\Delta\mathrm{Abs} = A\exp\left[-(kt)^{\beta}\right] \quad (3)$$

$$\bar{k}_{obs} = \left[\frac{1}{k\beta}\times\Gamma\left(\frac{1}{\beta}\right)\right]^{-1} \quad (4)$$

According to the results of CV experiments (Figure S1 in the Supporting Information), the $Ru^{III/II}$ redox potential of **2** is about 30 mV more positive than that of **3**. This means that the regeneration of $\mathbf{2}^+$ by iodide occurs with a larger driving force. The measured nearly twofold increase in the $k_{reg}$ is likely the result of this energetic difference. Under the open-circuit condition, a steady state concentration of $TiO_2(e^-)$ increases the charge recombination rate so that it can compete with the sensitizer regeneration.[15] A twofold slower regeneration rate would be responsible for the approximate 20 mV drop in $V_{oc}$ assuming the diode equation is applicable.[17]

## Conclusions

In summary, two novel tris-heteroleptic Ru–dipyrrinate complexes have been investigated as NCS-free sensitizers for DSSCs. Compared to the bis-heteroleptic complex **1**, complexes **2** and **3** possess enhanced light-harvesting ability, lower excited states reduction potentials, and much higher PCEs when used as DSSC dyes. The studies of electron injection yield and dye regeneration kinetics of **2**/$TiO_2$ and **3**/$TiO_2$ suggest the improved PCE is mainly due to **2** and **3** being stronger photoreductants, following the incorporation of electron-donating substituents into the ancillary bipyridine ligand. Although the efficiency of these two sensitizers is not optimal, the present study demonstrates that the performance of the Ru–dipyrrinate dyes can be substantially improved by the rational design of these molecular photosensitizers. To the best of our knowledge, this work represents the first report of the synthesis and functional use of tris-heteroleptic metal–dipyrrinate complexes and thus may serve as an encouragement to develop new classes of dipyrrinate-containing complexes as functional materials.

## Experimental Section

### Spectroscopic measurements

$^1$H NMR spectra were measured on a Bruker 600 MHz spectrometer. Chemical shifts were referenced to the residual proton signal in $CDCl_3$ (7.26 ppm). Electrospray ionization (ESI) mass spectra were acquired on a Beckman Coulter System Gold HPLC BioEssential with Binary Gradient 125S pump and a UV/Vis 166 analytical detector. Electronic absorption (UV/Vis) spectra were collected in the 300–1000 nm range on a Varian Cary 50Bio UV/Vis Spectrophotometer.

### Electrochemistry

Cyclic voltammograms (CV) were recorded on a CH Instruments 600D electrochemical analyzer at the sweep rate of 0.100 $Vs^{-1}$, with 0.100 M $(Bu_4N)PF_6$ in $CH_3CN$/DMF electrolyte solution, Pt working electrode, and $Ag^+$(0.01 M $AgNO_3$)/Ag reference electrode. All the potentials initially were referenced to the standard $Fc^+$/Fc couple (Fc = ferrocene), which was added as an internal standard upon completion of each CV experiment. The redox potentials reported in this work have been converted to the normal hydrogen electrode (NHE), assuming that the $Fc^+$/Fc couple has a redox potential of +0.630 V vs. NHE in $CH_3CN/CH_2Cl_2$. Spectroelectrochemical measurements were performed on a Varian Cary 50Bio UV/Vis spectrophotometer, using a commercial thin-layer cell with a Pt mesh electrode (BASi). The spectra were collected for various applied potentials after reaching redox equilibrium at each specific potential value.

### Theoretical calculations

Density functional theory (DFT) calculations were performed with the Gaussian 09 package, using the B3LYP hybrid functional and the DZVP basis set for Ru and the TZVP basis set for the other elements.[18] The spin-restricted and spin-unrestricted molecular orbital (MO) model was used for all closed- and open-shell species, respectively. All geometries were optimized in the ground state, without symmetry restraints, using the PCM implicit solvent model (with CH3OH as a solvent) to include solute-solvent interaction effects. Time-dependent (TD) DFT calculations in solution were carried out on the optimized geometries. Compositions of molecular orbitals were analyzed using the AOMix software.[19]

### Cell fabrication

Photoanodes were prefabricated by Dyesol, Inc. (Australia) with a screen-printable $TiO_2$ pastes (18-NRT, Dyesol). The active area of the $TiO_2$ electrode was 0.28 $cm^2$ with a thickness of 12 μm (18-NRT) and 3 μm of scattering layer on fluorine-doped tin-oxide (FTO; TEC15 (15 $\Omega\,cm^{-2}$)). $TiO_2$ substrates were treated with an aqueous solution of $TiCl_4$ (0.05 M) for 30 min at 70 °C and subsequently rinsed with $H_2O$ and dried prior to heating. The electrodes were heated to 450 °C for 20 min under ambient atmosphere and allowed to cool to 80 °C before dipping them into the dye solution. The anode was soaked overnight for 16 h in a dye-containing $CH_3OH$ solution (~0.25 mM). The stained films were rinsed copiously with the solvent, in which they were dipped, and subsequently dried. The cells were fabricated using a Pt-coated counter-electrode (FTO TEC-15 (15 $\Omega\,cm^{-2}$)) and sandwiched with a 30 μm Surlyn (Dupont) gasket by resistive heating. An electrolyte solution, containing 0.7 M LiI, 0.06 M $I_2$, 0.3 M 1,3-dimethylimidazolium iodide, and 0.1 M guanidinium thiocyanate in $CH_3CN$/valeronitrile (85:15 v/v), was introduced into the void via vacuum backfilling through a hole in the counter electrode. The hole was sealed with an aluminum-backed Bynel foil (Dyesol). After sealing, silver bus bars were added to all cells.

### Cell characterization

Photovoltaic measurements were performed with a Newport Oriel solar simulator (Model 9225 A1) equipped with a class A 150 W xenon light source powered by a Newport power supply (Model 69907). The light output (area = 5 × 5 $cm^2$) was calibrated to AM1.5 using a Newport Oriel correction filter to reduce the spectral mismatch in the region of 350–700 nm to less than 1.5%. The power output of the lamp was measured to 1 Sun (100 $mW\,cm^{-2}$) using a certified Si reference cell. The current–voltage (*I–V*) characteristic of each cell was obtained by applying an external potential bias to the cell and measuring the generated photocurrent with a Keithley digital source meter (Model 2400). All cells were measured with a mask size of 0.88 $cm^2$. IPCE measurements were performed on a QEX7 Solar Cell Spectral Response Measurement System (PV Instruments, Inc.) equipped with a photodiode that was calibrated against NIST standard I755 with transfer uncertainty less than 0.5% between 400–1000 nm and less than 1% at all other wavelengths. All measurements were made in AC mode at 4 Hz chopping frequency under a bias light between 0.01 to 0.1 Sun. The system was calibrated and operated in Beam Power mode.

### Substrate preparation for spectroscopy

Mesoporous nanocrystalline $TiO_2$ thin films were prepared as previously described.[20] Briefly, $TiO_2$ paste was prepared by acid hydrolysis of [Ti(O*i*Pr)$_4$] (Aldrich, 97%) using a sol-gel technique. The paste was cast onto the transparent FTO conductive substrate (Hartford Glass 15 Ω/sq) by doctor blade and annealed at 450 °C for 30 min under constant flow of $O_2$. The $TiO_2$/FTO films were immersed in a 40 mM aqueous solution of $TiCl_4$ at 70 °C for 30 min and rinsed with de-ionized water. The films were then sintered again under the same conditions as described above. The films so prepared were immersed in $CH_3OH$ solutions of the dyes that contained about 1 molar equivalent of $(Bu_4N)OH$. The surface coverage was controlled by the immersion time to obtain the optimal optical density for transient absorption measurements. The sensitized films were rinsed with $CH_3OH$ and $CH_3CN$, and diagonally positioned in a standard 1 $cm^2$ quartz cuvette containing 0.5 M solution of $LiClO_4$ in $CH_3CN$. The electrolyte solutions were purged with Ar gas for at least 30 min prior to experimentation.

### Transient absorption spectroscopy

Nanosecond TA measurements were performed with an apparatus similar to the one previously described.[20] Briefly, the samples were excited at 45° to the film by a Q-switched, pulsed Nd:YAG laser (Quantel USA (BigSky) Brilliant B; 5–6 ns full width at half-maximum, 1 Hz, ~10 mm in diameter) at 532 nm (frequency doubled). A 150 W Xenon arc lamp coupled to a 1/4 m monochromator (Spectral Energy, Corp. GM 252) served as the probe beam (Applied Photophysics) that was aligned orthogonally to the excitation light. Detection was achieved with a monochromator (Spex 1702/04) optically coupled to an R928 photomultiplier tube (Hamamatsu). Approximately 150–250 laser pulses were typically averaged for each single wavelength measurement to achieve satisfactory signal-to-noise ratios. Kinetic data fitting was performed in Origin 8, and least-squares error minimization was accomplished using the Levenberg-Marquardt iteration method.

### Syntheses

All reactions were performed under inert ($N_2$) atmosphere using standard Schlenk techniques, unless noted otherwise. All reagents were purchased from Aldrich, except for $RuCl_3{\cdot}3H_2O$ (Pressure Chemical Company), pyrrole (Alfa Aesar), and α-phellandrene (TCI). All reagents were used as received, except for pyrrole which was distilled prior to use. 4,4′-bis(ethoxycarbonyl)-2,2′-bipyridine (deeb),[21] 4,4′-bis(5-hexylthiophene-2-yl)-2,2′-bipyridine,[2d] 4,4′-bis(5-hexyl-3,4-ethylenedioxythiophene-2-yl)-2,2′-bipyridine[14] and [(*p*-cymene)Ru(2-TDP)Cl][4] were prepared according to published procedures. Anhydrous commercial solvents were additionally purified by passing through a double-stage drying/purification system (Glass Contour Inc.).

**[Ru(2-TDP)($CH_3CN$)$_4$]$NO_3$**: A mixture of [(*p*-cymene)Ru(2-TDP)Cl] (500 mg, 1.01 mmol) and $AgNO_3$ (175 mg, 1.03 mmol) in anhydrous $CH_3CN$ (30 mL) was heated at reflux for 4 days under reduced light. After cooling down to room temperature (RT), the reaction mixture was filtered through Celite to remove AgCl and the filtrate was concentrated to dryness under reduced pressure. The crude product was loaded on a neutral alumina column (3 cm × 18 cm) and washed with a mixture of $CH_2Cl_2$:$CH_3OH$ (30:1 v/v). After removing a bright orange band, the eluent was changed to $CH_2Cl_2$:$CH_3OH$ (10:1 v/v) and the major dark orange band was collected and dried under reduced pressure to afford 479 mg of orange-brown solid (yield = 86%). $^1$H NMR ($CDCl_3$, 600 MHz): $\delta$ = 7.81 (t, $J$ = 1.4 Hz, 2H), 7.47 (dd, $J$ = 5.1, 1.2 Hz, 1H), 7.29 (dd, $J$ = 3.5, 1.2 Hz, 1H), 7.12 (dd, $J$ = 5.1, 3.5 Hz, 1H), 6.97 (dd, $J$ = 4.4, 1.3 Hz, 2H), 6.49 (dd, $J$ = 4.4, 1.4 Hz, 2H), 2.87 (s, 6H), 2.30 ppm (s, 6H); $^{13}$C NMR (CDCl3, 151 MHz): $\delta$ = 152.01, 139.22, 138.73, 136.46, 131.52, 130.37,

126.80, 126.42, 124.12, 120.99, 117.51, 5.56, 4.69 ppm; HR-ESI-MS: *m/z* calcd for $[Ru(2\text{-}TDP)(CH_3CN)_4]^+$: 491.05919; found: 491.05952.

**$[Ru(deeb)(2\text{-}TDP)(CH_3CN)_2]NO_3$**: A mixture of $[Ru(2\text{-}TDP)(CH_3CN)_4]NO_3$ (300 mg, 0.54 mmol) and deeb (163 mg, 0.54 mmol) in anhydrous EtOH (150 mL) was heated at 55 °C for 30 h. After cooling down to RT, the solvent was removed under reduced pressure. The crude product was loaded on a silica column (2.5 cm × 20 cm) and washed with a mixture of $CH_2Cl_2$:$CH_3OH$ (15:1 v/v). After removing several fast-moving impurity bands, $[Ru(deeb)_2(2\text{-}TDP)]NO_3$ appeared as a maroon band closely followed by a grey band of the desired product ($R_f$ = 0.25). The latter was collected and dried under reduced pressure to afford 200 mg of brown solid (yield = 48%). $^1$H NMR ($CDCl_3$, 600 MHz): $\delta$ = 9.15 (d, $J$ = 5.7 Hz, 2H), 8.96 (s, 2H), 8.19 (d, $J$ = 5.6 Hz, 2H), 7.93 (s, 2H), 7.54 (dd, $J$ = 5.2, 1.1 Hz, 1H), 7.42 (dd, $J$ = 3.5, 1.1 Hz, 1H), 7.21 (dd, $J$ = 4.9, 1.7 Hz, 2H), 6.67–6.64 (dd, $J$ = 4.2, 1.2 Hz, 2H), 4.56 (q, $J$ = 7.1 Hz, 4H), 2.21 (s, 6H), 1.51 ppm (t, $J$ = 7.1 Hz, 6H); $^{13}$C NMR ($CDCl_3$, 151 MHz): $\delta$ = 163.86, 159.60, 154.65, 153.41, 139.49, 139.26, 138.80, 137.94, 131.98, 130.71, 127.43, 127.16, 124.37, 122.49, 121.92, 117.68, 63.00, 14.47, 4.69 ppm; HR-ESI-MS: *m/z* calcd for $[Ru(deeb)(2\text{-}TDP)(CH_3CN)_2]^+$: 709.13960; found: 709.11248.

**$[Ru(deeb)(2\text{-}TDP)(dthbpy)]NO_3$ (2a)**: A mixture of $[Ru(deeb)(2\text{-}TDP)(CH_3CN)_2]NO_3$ (100 mg, 0.13 mmol) and dthbpy (70 mg, 0.14 mmol) in anhydrous EtOH (20 mL) was heated at reflux for 48 h. After cooling down to RT, the solvent was removed under reduced pressure. The crude product was loaded on a silica column (2.5 cm × 20 cm) and washed with $CH_2Cl_2$:$CH_3OH$ (15:1 v/v). After removing several fast-moving impurity bands, the major maroon band ($R_f$ = 0.30) was collected and dried in vacuum to afford 100 mg of dark red solid (yield = 80%). $^1$H NMR ($CDCl_3$, 400 MHz): $\delta$ = 9.22 (d, $J$ = 1.7 Hz, 1H), 9.18 (d, $J$ = 1.6 Hz, 1H), 8.83 (s, 2H), 8.34 (d, $J$ = 3.8 Hz, 1H), 8.28 (d, $J$ = 3.8 Hz, 1H), 8.12 (d, $J$ = 5.9 Hz, 2H), 7.87 (t, $J$ = 5.9 Hz, 2H), 7.63 (d, $J$ = 6.1 Hz, 1H), 7.49 (dd, $J$ = 5.1 Hz, 1.2, 1H), 7.40–7.33 (m, 3H), 7.29 (dd, $J$ = 3.5 Hz, 1.1 Hz, 1H), 7.13–7.11 (m, 1H), 7.01 (d, $J$ = 1.2 Hz, 1H), 7.00 (d, $J$ = 1.2 Hz, 1H), 6.94–6.90 (m, 2H), 6.55 (t, $J$ = 1.3 Hz, 1H), 6.37 (dd, $J$ = 4.4 Hz, 1.4 Hz, 1H), 6.25–6.24 (m, 2H), 4.53–4.45 (m, 4H), 2.87–2.79 (m, 4H), 1.74–1.63 (m, 4H), 1.47–1.41 (m, 6H), 1.32–1.28 (m, 12H), 0.92–0.86 ppm (m, 6H); $^{13}$C NMR ($CDCl_3$, 101 MHz): $\delta$ = 163.90, 163.78, 158.93, 158.28, 157.83, 156.82, 153.09, 151.93, 150.83, 150.70, 150.50, 150.25, 149.92, 148.72, 143.67, 143.19, 139.76, 139.03, 136.42, 136.34, 136.10, 135.85, 135.73, 132.79. 131.79, 131.09, 130.88, 130.30, 127.38, 127.27, 126.41, 126.28, 125.58, 122.57, 120.12, 119.22, 118.25, 62.87, 62.76, 31.64, 31.62, 31.54, 30.54, 28.82, 28.79, 28.06, 27.00, 22.68, 22.66, 14.41, 14.35, 14.19, 14.17, 13.75 ppm; HR-ESI-MS: *m/z* calcd for $[Ru(deeb)(2\text{-}TDP)(dthbpy)]^+$: 1115.29599; found: 1115.29844.

**$[Ru(deeb)(2\text{-}TDP)(bis\text{-}EDOT\text{-}bpy)]NO_3$ (3a)**: A mixture of $[Ru(deeb)(2\text{-}TDP)(CH_3CN)_2]NO_3$ (140 mg, 0.18 mmol) and bis-EDOT-bpy (120 mg, 0.20 mmol) in anhydrous EtOH (20 mL) was heated at reflux for 40 h. After cooling down to RT, the solvent was removed under reduced pressure. The crude product was loaded on a silica column (2.5 cm × 20 cm) and washed with $CH_2Cl_2$:$CH_3OH$ (15:1 v/v). After removing several fast-moving impurity bands, the major maroon band ($R_f$ = 0.30) was collected and dried under reduced pressure affording 210 mg of dark red solid (yield = 90%). $^1$H NMR ($CDCl_3$, 700 MHz): $\delta$ = 8.84 (t, $J$ = 1.5 Hz, 2H), 8.56 (d, $J$ = 1.9 Hz, 1H), 8.49 (d, $J$ = 1.9 Hz, 1H), 8.12 (d, $J$ = 6.0 Hz, 1H), 8.06 (d, $J$ = 6.0 Hz, 1H), 7.87 (t, $J$ = 1.5 Hz, 1H), 7.86 (t, $J$ = 1.5 Hz, 1H), 7.58 (d, $J$ = 6.2 Hz, 1H), 7.49 (t, $J$ = 1.4 Hz, 1H), 7.48–7.47 (m, 1H), 7.39 (dd, $J$ = 6.2, 2.0 Hz, 1H), 7.30 (d, $J$ = 6.2 Hz, 1H), 7.27 (dd, $J$ = 3.5, 1.2 Hz, 1H), 7.11 (dd, $J$ = 5.1, 3.5 Hz, 1H), 7.00 (dd, $J$ = 4.5, 1.3 Hz, 1H), 6.91 (dd, $J$ = 4.4, 1.3 Hz, 1H), 6.51 (t, $J$ = 1.5 Hz, 1H), 6.35 (dd, $J$ = 4.5, 1.5 Hz, 1H), 6.25 (dd, $J$ = 4.4, 1.6 Hz, 1H), 6.23 (t, $J$ = 1.5 Hz, 1H), 4.55–4.44 (m, 4H), 4.36 (dt, $J$ = 6.0, 3.0 Hz, 2H), 4.33 (dt, $J$ = 5.4, 3.0 Hz, 2H), 2.73–2.69 (m, 2H), 2.67 (t, $J$ = 7.6 Hz, 2H), 1.62 (dt, $J$ = 21.4, 7.5 Hz, 4H), 1.43 (dt, $J$ = 13.2, 7.1 Hz, 6H), 1.39–1.25 (m, 12H), 0.90–0.84 ppm (m, 6H); $^{13}$C NMR ($CDCl_3$, 176 MHz): $\delta$ = 163.80, 163.63, 159.04, 158.17, 157.26, 156.14, 153.12, 151.53, 150.75, 149.80, 149.62, 148.92, 143.88, 143.51, 142.20, 142.03, 141.58, 139.87, 139.10, 138.99, 138.90, 136.47, 136.31, 135.89, 135.78, 132.72, 132.05, 130.91, 127.34, 126.43, 126.15, 125.67, 123.95, 123.54, 122.61, 122.37, 121.42, 121.34, 118.99, 118.45, 118.04, 117.81, 108.54, 108.22, 66.07, 66.01, 64.54, 62.97, 62.84, 31.58, 31.55, 30.17, 28.83, 28.81, 28.31, 27.08, 26.24, 22.66, 22.64, 14.40, 14.37, 14.17, 14.16, 13.85 ppm; HR-ESI-MS: *m/z* calcd for $[Ru(deeb)(2\text{-}TDP)(bis\text{-}EDOT\text{-}bpy)]^+$: 1231.30695; found: 1231.30188.

**$[Ru(Hdcbpy)(2\text{-}TDP)(dthbpy)]$ (2)**: A solution of **2a** (70 mg, 0.06 mmol) in of DMF:$NEt_3$:$H_2O$ (3:1:1 v/v/v; 15 mL) was heated at reflux for 18 h. After cooling down to RT, the volatiles were removed under reduced pressure and $CH_3CN$ (30 mL) was added to remove unreacted starting materials and byproducts. The obtained product was washed with diethyl ether and dried in vacuum to afford 53 mg of black powder (yield = 84%). $^1$H NMR ($CDCl_3$, 600 MHz): $\delta$ = 10.00 (s, 2H), 8.25 (d, $J$ = 15.6 Hz, 2H), 7.95 (s, 2H), 7.90 (s, 1H), 7.82 (d, $J$ = 6.1 Hz, 1H), 7.76 (d, $J$ = 4.8 Hz, 1H), 7.56–7.42 (m, 4H), 7.31 (d, $J$ = 12.2 Hz, 2H), 7.12 (s, 1H), 6.96 (d, $J$ = 13.3 Hz, 2H), 6.89 (s, 1H), 6.86 (s, 1H), 6.49 (s, 1H), 6.40 (s, 1H), 6.32 (d, $J$ = 4.1 Hz, 1H), 6.29 (s, 1H), 2.88 (dd, $J$ = 15.9, 8.2 Hz, 4H), 1.72 (dt, $J$ = 15.3, 7.4 Hz, 4H), 1.45–1.27 (m, 12H), 1.00–0.78 ppm (m, 6H); HR-ESI-MS: *m/z* calcd for $[Ru(H_2dcbpy)(2\text{-}TDP)(dthbpy)]^+$: 1059.23339; found: 1059.23609; elemental analysis calcd (%) for $RuS_3O_7N_6C_{55}H_{58}$ (**1**·3 $H_2O$): C 59.39, H 5.26, N 7.56; found: C 59.00, H 5.03, N 7.43.

**$[Ru(Hdcbpy)(2\text{-}TDP)(bis\text{-}EDOT\text{-}bpy)]$ (3)**: The dye was prepared in a fashion similar to that described for **2**, using **3a** (150 mg, 0.12 mmol) as starting material. Yield = 91%. $^1$H NMR ($CDCl_3$, 600 MHz), $\delta$ = 9.78 (s, 2H), 8.42 (s, 1H), 8.35 (s, 1H), 8.05–8.00 (m, 1H), 7.94 (d, $J$ = 4.9 Hz, 1H), 7.91 (d, $J$ = 6.2 Hz, 1H), 7.85 (d, $J$ = 6.0 Hz, 1H), 7.68 (d, $J$ = 6.1 Hz, 1H), 7.56 (d, $J$ = 6.1 Hz, 1H), 7.48 (d, $J$ = 5.3 Hz, 2H), 7.36 (d, $J$ = 6.1 Hz, 1H), 7.30 (s, 1H), 7.13–7.10 (m, 1H), 6.98 (d, $J$ = 3.7 Hz, 1H), 6.93 (d, $J$ = 3.9 Hz, 1H), 6.53 (s, 1H), 6.35 (s, 1H), 6.33 (d, $J$ = 5.1 Hz, 1H), 6.27 (d, $J$ = 3.9 Hz, 1H), 4.41 (d, $J$ = 25.1 Hz, 4H), 4.30 (d, $J$ = 22.3 Hz, 4H), 2.70 (dt, $J$ = 18.3, 7.2 Hz, 4H), 1.64 (tt, $J$ = 15.5, 7.4 Hz, 4H), 1.43–1.26 (m, 12H), 0.89 ppm (dd, $J$ = 12.5, 6.7 Hz, 6H); HR-ESI-MS: *m/z* calcd for $[Ru(H_2dcbpy)(2\text{-}TDP)(bis\text{-}EDOT\text{-}bpy)]^+$: 1175.24435; found: 1175.24485; elemental analysis calcd (%) for $RuS_3O_{10}N_6C_{59}H_{60}$ (**3**·2 $H_2O$): C 58.55, H 5.00, N 6.94; found: C 58.76, H 5.03, N 7.05.

## Acknowledgements

This research was supported in part by a grant from the Council on Research and Creativity at Florida State University.

**Keywords:** dyes/pigments · dye-sensitized solar cells · injection yield · N ligands · ruthenium

[1] M. Grätzel, *Inorg. Chem.* **2005**, *44*, 6841 – 6851.

[2] a) M. K. Nazeeruddin, A. Kay, I. Rodicio, R. Humphry-Baker, E. Mueller, P. Liska, N. Vlachopoulos, M. Grätzel, *J. Am. Chem. Soc.* **1993**, *115*, 6382 – 6390; b) P. Péchy, T. Renouard, S. M. Zakeeruddin, R. Humphry-Baker, P. Comte, P. Liska, L. Cevey, E. Costa, V. Shklover, L. Spiccia, G. B. Deacon, C. A. Bignozzi, M. Grätzel, *J. Am. Chem. Soc.* **2001**, *123*, 1613 – 1624; c) F. Gao, Y. Wang, J. Zhang, D. Shi, M. Wang, R. Humphry-Baker, P. Wang,

 

S. M. Zakeeruddin, M. Grätzel, *Chem. Commun.* **2008**, 2635 – 2637; d) F. Gao, Y. Wang, D. Shi, J. Zhang, M. Wang, X. Jing, R. Humphry-Baker, P. Wang, S. M. Zakeeruddin, M. Grätzel, *J. Am. Chem. Soc.* **2008**, *130*, 10720 – 10728.

[3] a) T. Bessho, E. Yoneda, J. H. Yum, M. Guglielmi, I. Tavernelli, H. Imai, U. Rothlisberger, M. K. Nazeeruddin, M. Grätzel, *J. Am. Chem. Soc.* **2009**, *131*, 5930 – 5934; b) P. G. Bomben, T. J. Gordon, E. Schott, C. P. Berlinguette, *Angew. Chem. Int. Ed.* **2011**, *50*, 10682 – 10685; *Angew. Chem.* **2011**, *123*, 10870 – 10873; c) C.-C. Chou, K.-L. Wu, Y. Chi, W.-P. Hu, S. J. Yu, G.-H. Lee, C.-L. Lin, P.-T. Chou, *Angew. Chem. Int. Ed.* **2011**, *50*, 2054 – 2058; *Angew. Chem.* **2011**, *123*, 2102 – 2106; d) K. C. D. Robson, B. D. Koivisto, A. Yella, B. Sporinova, M. K. Nazeeruddin, T. Baumgartner, M. Grätzel, C. P. Berlinguette, *Inorg. Chem.* **2011**, *50*, 5494 – 5508.

[4] G. Li, P. G. Bomben, K. C. D. Robson, S. I. Gorelsky, C. P. Berlinguette, M. Shatruk, *Chem. Commun.* **2012**, *48*, 8790 – 8792.

[5] G. Li, K. Hu, C. Yi, K. L. Knappenberger, G. J. Meyer, S. I. Gorelsky, M. Shatruk, *J. Phys. Chem. C* **2013**, *117*, 17399 – 17411.

[6] a) L. Yu, K. Muthukumaran, I. V. Sazanovich, C. Kirmaier, E. Hindin, J. R. Diers, P. D. Boyle, D. F. Bocian, D. Holten, J. S. Lindsey, *Inorg. Chem.* **2003**, *42*, 6629 – 6647; b) T. E. Wood, A. Thompson, *Chem. Rev.* **2007**, *107*, 1831 – 1861.

[7] M. Myahkostupov, F. N. Castellano, *Inorg. Chem.* **2011**, *50*, 9714 – 9727.

[8] P. G. Bomben, K. D. Thériault, C. P. Berlinguette, *Eur. J. Inorg. Chem.* **2011**, 1806 – 1814.

[9] a) S. J. Smalley, M. R. Waterland, S. G. Telfer, *Inorg. Chem.* **2009**, *48*, 13 – 15; b) G. Li, L. Ray, E. N. Glass, K. Kovnir, A. Khoroshutin, S. I. Gorelsky, M. Shatruk, *Inorg. Chem.* **2012**, *51*, 1614 – 1624.

[10] a) J. V. Caspar, B. P. Sullivan, E. M. Kober, T. J. Meyer, *Chem. Phys. Lett.* **1982**, *91*, 91 – 95; b) E. M. Kober, J. V. Caspar, R. S. Lumpkin, T. J. Meyer, *J. Phys. Chem.* **1986**, *90*, 3722 – 3734.

[11] I. V. Sazanovich, C. Kirmaier, E. Hindin, L. Yu, D. F. Bocian, J. S. Lindsey, D. Holten, *J. Am. Chem. Soc.* **2004**, *126*, 2664 – 2665.

[12] A. A. Vlcek, E. S. Dodsworth, W. J. Pietro, A. B. P. Lever, *Inorg. Chem.* **1995**, *34*, 1906 – 1913.

[13] a) G. Boschloo, E. A. Gibson, A. Hagfeldt, *J. Phys. Chem. Lett.* **2011**, *2*, 3016 – 3020; b) K. C. D. Robson, P. G. Bomben, C. P. Berlinguette, *Dalton Trans.* **2012**, *41*, 7814 – 7829.

[14] J.-J. Kim, H. Choi, S. Paek, C. Kim, K. Lim, M.-J. Ju, H. S. Kang, M.-S. Kang, J. Ko, *Inorg. Chem.* **2011**, *50*, 11340 – 11347.

[15] a) K. C. D. Robson, K. Hu, G. J. Meyer, C. P. Berlinguette, *J. Am. Chem. Soc.* **2013**, *135*, 1961 – 1971; b) F. Li, J. R. Jennings, Q. Wang, *ACS Nano* **2013**, *7*, 8233 – 8242.

[16] a) G. Williams, D. C. Watts, *Trans. Faraday Soc.* **1970**, *66*, 80 – 85; b) C. P. Lindsey, G. D. Patterson, *J. Chem. Phys.* **1980**, *73*, 3348 – 3357.

[17] A. Kumar, P. G. Santangelo, N. S. Lewis, *J. Phys. Chem.* **1992**, *96*, 834 – 842.

[18] Gaussian 09, Revision A.02, M. J. Frisch, G. W. Trucks, H. B. Schlegel, G. E. Scuseria, M. A. Robb, J. R. Cheeseman, G. Scalmani, V. Barone, B. Mennucci, G. A. Petersson, H. Nakatsuji, M. Caricato, X. Li, H. P. Hratchian, A. F. Izmaylov, J. Bloino, G. Zheng, J. L. Sonnenberg, M. Hada, M. Ehara, K. Toyota, R. Fukuda, J. Hasegawa, M. Ishida, T. Nakajima, Y. Honda, O. Kitao, H. Nakai, T. Vreven, J. A. Montgomery, Jr., J. E. Peralta, F. Ogliaro, M. Bearpark, J. J. Heyd, E. Brothers, K. N. Kudin, V. N. Staroverov, R. Kobayashi, J. Normand, K. Raghavachari, A. Rendell, J. C. Burant, S. S. Iyengar, J. Tomasi, M. Cossi, N. Rega, J. M. Millam, M. Klene, J. E. Knox, J. B. Cross, V. Bakken, C. Adamo, J. Jaramillo, R. Gomperts, R. E. Stratmann, O. Yazyev, A. J. Austin, R. Cammi, C. Pomelli, J. W. Ochterski, R. L. Martin, K. Morokuma, V. G. Zakrzewski, G. A. Voth, P. Salvador, J. J. Dannenberg, S. Dapprich, A. D. Daniels, Ö. Farkas, J. B. Foresman, J. V. Ortiz, J. Cioslowski, D. J. Fox, Gaussian, Inc. Wallingford CT, **2009**..

[19] S. I. Gorelsky in *AOMix: Program for molecular orbital analysis*, Version 6.5, University of Ottawa: Ottawa, Canada, **2011**; http://www.sgchem.net/.

[20] R. Argazzi, C. A. Bignozzi, T. A. Heimer, F. N. Castellano, G. J. Meyer, *Inorg. Chem.* **1994**, *33*, 5741 – 5749.

[21] K. Wiederholt, L. W. McLaughlin, *Nucleic Acids Res.* **1999**, *27*, 2487 – 2493.

Received: September 13, 2014
Published online on November 28, 2014